Am. J. Trop. Med. Hyg., 97(2), 2017, pp. 548–555
doi:10.4269/ajtmh.16-0742

Case Report: Severe and Complicated Cynomolgi Malaria in a Rhesus Macaque Resulted in Similar Histopathological Changes as Those Seen in Human Malaria

Chester J. Joyner,[1] The MaHPIC Consortium,[1] Jennifer S. Wood,[5] Alberto Moreno,[1,2,3] Anapatricia Garcia,[4] and Mary R. Galinski[1,2,3]*

[1]*Malaria Host–Pathogen Interaction Center, Emory Vaccine Center, Yerkes National Primate Research Center, Emory University, Atlanta, Georgia;* [2]*Emory Vaccine Center, Yerkes National Primate Research Center, Emory University, Atlanta, Georgia;* [3]*Division of Infectious Diseases, Department of Medicine, Emory University, Atlanta, Georgia;* [4]*Division of Pathology, Yerkes National Primate Research Center, Emory University, Atlanta, Georgia;* [5]*Division of Animal Resources, Yerkes National Primate Research Center, Emory University, Atlanta, Georgia*

Abstract. Histopathological data collected from patients with severe malaria have been instrumental for studying malaria pathogenesis. Animal models of malaria are critical to complement such studies. Here, the histopathological changes observed in a rhesus macaque with severe and complicated *Plasmodium cynomolgi* malaria are reported. The animal presented with thrombocytopenia, severe anemia, and hyperparasitemia during the acute infection. The macaque was given subcurative antimalarial treatment, fluid support, and a blood transfusion to treat the clinical complications, but at the time of transfusion, kidney function was compromised. These interventions did not restore kidney function, and the animal was euthanized due to irreversible renal failure. Gross pathological and histological examinations revealed that the lungs, kidneys, liver, spleen, and bone marrow exhibited abnormalities similar to those described in patients with malaria. Overall, this case report illustrates the similarities in the pathophysiological complications that can occur in human malaria and cynomolgi malaria in rhesus macaques.

INTRODUCTION

Clinical malaria presents with a variety of signs and symptoms that range from asymptomatic to life threatening, but the factors and mechanisms that result in this spectrum of disease severity are largely unknown.[1–4] Tissues collected at autopsy from humans who have succumbed to falciparum malaria have been informative for studies on severe and complicated malaria pathogenesis as well as parasite biology.[5–7] Non-human primate (NHP) and rodent malaria models have complemented these studies by enabling investigations of mechanisms that cannot be directly studied using patient samples or postmortem tissues.[8–10] Similarly, studies using tissues collected from patients with vivax malaria have provided insight into vivax malaria pathophysiology.[2,11,12] Complementary studies using animal models would greatly enhance the ability to study vivax malaria pathogenesis. However, rodent models of vivax malaria do not exist, and NHP models of vivax malaria have been underutilized.[13,14]

The *Plasmodium cynomolgi*–rhesus macaque model of *Plasmodium vivax* infection mimics the hematological changes and clinical presentations observed in patients with vivax malaria.[15] In addition, *P. cynomolgi* shares many biological characteristics with *P. vivax* including genetic makeup,[16] infected red blood cell (RBC) structures such as caveola–vesicle complexes,[17,18] preferential invasion of reticulocytes,[19] and formation of hypnozoites.[20,21] These factors make this model system ideal for studying vivax malaria and determining if and which pathophysiological mechanisms are shared between vivax malaria in humans and cynomolgi malaria in rhesus macaques.

In this case report, the histopathological changes associated with severe and complicated cynomolgi malaria in a rhesus monkey are described for the first time to our knowledge.

* Address correspondence to Mary R. Galinski, Division of Infectious Diseases, Department of Medicine, Emory University, Atlanta, GA. E-mail: mgalins@emory.edu

MATERIALS AND METHODS

Experimental design. A case of severe and complicated malaria in an animal from a cohort of five *Macaca mulatta* (Indian rhesus macaques) experimentally infected with *P. cynomolgi* M/B strain[22] is presented here. A detailed description of the experimental procedures, animal housing, enrichment activities, clinical interventions, hematological parameters, and clinical outcomes has been reported previously.[15]

Animal use. This study was approved by Emory University's Institutional Animal Care and Use Committee (IACUC). All endpoints, including humane euthanasia, were documented and approved. Regular consulting with Yerkes National Primate Research Center veterinarians and staff was done throughout the experiment.

Blood chemistry. Blood was collected in a heparinized tube at the time of transfusion and analyzed using a Liasys serum chemistry automated analyzer.

Gross pathology and histological analysis. Complete postmortem evaluation of this rhesus macaque was performed after IACUC approved humane euthanasia. Organs from this animal were collected shortly after gross pathological examination. Sections of main organ tissues were collected and fixed in 10% buffered formalin and processed for routine histological evaluation following hematoxylin and eosin staining.[23] In addition, selected organ sections were stained with Masson's Trichrome blue or Pearl's iron stain using standard methodologies.[23]

Transmission electron microscopy. Selected tissue sections collected at the time of necropsy were processed for transmission electron microscopy (TEM) as previously described and evaluated using a JEM 1210 electron microscope (Peabody, MD).[24]

Data deposition. Serum blood chemistry profiles are publicly available on PlasmoDB.[25]

RESULTS

Clinical presentation. The hematological and parasitological data related to this animal were previously presented

in Joyner et al. but is summarized below.[15] A group of five rhesus macaques were experimentally infected with 2,000 freshly isolated *P. cynomolgi* M/B strain sporozoites via intravenous injection on day 0, and the infection reached patency 12 days post-inoculation (PI). On day 19 PI, one animal presented with hyperparasitemia, 1,214,842 parasites/μL or 19.95%, and thrombocytopenia (< 150,000 platelets/μL).[15] A subcurative, blood-stage treatment using artemether (dose: 1 mg/kg) was subsequently administered intramuscularly on day 21 PI to reduce parasitemia. On day 22 PI, the parasitemia decreased after administration of artemether; however, hemoglobin dropped to 6.8 g/dL. The animal was given a whole blood transfusion to treat severe anemia, and at the time of transfusion, the serum chemistry profile was determined. Liver dysfunction was evident based on elevated serum aspartate aminotransferase (AST) and alanine aminotransferase (ALT) concentrations (Table 1). Kidney dysfunction was also apparent based on elevated serum blood urea nitrogen, creatinine, and potassium in addition to decreased sodium concentrations (Table 1). On day 23 PI, the animal's condition had not improved despite veterinary interventions and supportive care (Table 1), and humane euthanasia was performed by intravascular pentobarbital overdose.

Physical examination. The animal weighed 6.27 kg at the time of necropsy, and the physical appearance was fair. The mucous membranes were pale and had a yellow tint (data not shown).

Gross pathology. Hepatosplenomegaly was evident with the spleen weighing 26.4 g, approximately eight times the normal weight, and the liver weighing 207.4 g, about double the normal weight. Both had a bronze discoloration (Figure 1A and data not shown). The lungs were pale and discolored with a green tint (Figure 3A). The kidneys were enlarged, swollen, and also discolored (Figure 5A). On sectioning, the kidneys were wet and congested in the medullary regions. Fluid was present in the abdomen. The alimentary canal, heart, skull, brain, bone marrow, joints, lymph nodes, pelvic organs, urinary bladder, and adrenals appeared normal (data not shown).

Histopathology. The spleen contained many macrophages with brown–black pigment that were negative for iron stain. This finding, consistent with the presence of hemozoin, was confirmed by TEM (Figure 1B–C). Interestingly, a macrophage-containing hemozoin also appears to have phagocytosed an uninfected RBC (Figure 1E). Other splenic structures such as lymphoid follicles and periarteriolar lymphatic sheaths appeared morphologically normal (Figure 1B).

The bone marrow was moderately hypercellular (Figure 2A). Myeloid and erythroid cell lineages were present, although erythroid precursors were markedly increased (Figure 2A). Intriguingly, megakaryocytes were enlarged, dysplastic, and possessed multiple misshapen nuclei (Figure 2C and D). Hemozoin was scattered throughout the marrow and appeared to be contained within macrophages (Figure 2B).

The lungs showed signs of edema and interstitial pneumonia (Figure 3B). Multifocal areas of type II cell hyperplasia were observed, and some areas of the alveolar walls appeared mildly thickened with fibrin (Figure 3C and F). TEM revealed that the pulmonary interstitium contained filamentous structures consistent with fibrin deposition (Figure 3F and G). The alveolar walls had macrophages containing an electron-dense crystalloid material, consistent with hemozoin (Figure 3C and D).

The liver contained multiple areas of inflammatory infiltrates composed of plasma cells and lymphocytes; this was particularly evident in the portal areas (Figure 4C). The hepatocytes were vacuolated and occasionally appeared eosinophilic (Figure 4A). The sinusoids were lined by hemozoin-containing macrophages, likely Kupffer cells

TABLE 1

Blood chemistry values of a rhesus macaque with severe and complicated cynomolgi malaria at the time of clinical intervention and 24 hours after

Analyte	Reference range	Before clinical intervention	24 hours after clinical intervention
Total protein	7.8–9.6	5.6	5.9
Albumin	3.1–5.3	2.7	3
Globulin	1.5–7	2.9	2.9
Albumin/Globulin ratio	1–100	0.9	1
AST	14–30 μ/L	57	72
ALT	14–30 μ/L	152	114
Alkaline phosphatase	100–277	228	385
Gamma glutamyl transferase	14–75	40	68
Bilirubin	0–3.7	0.3	0.2
BUN	8–30 mg/dL	180	171
Creatinine	0.8–2.3 mg/dL	8.3	8.6
Blood urea nitrogen/creatinine ratio	1–25	21.8	22.3
Phosphorus	3.5–6.5	6.8	9.1
Glucose	84–131 mg/dL	93	77
Calcium	9.8–11.8 mg/dL	8.7	8.7
Magnesium	0.3–5	2	2.3
Sodium	142–160	130	134
Potassium	4.1–5.3	5.7	5.5
Chloride	97–113	93	99
Cholesterol	97–186	163	177
Triglycerides	0–800	560	605
Amylase	88–400	379	477
Creatine phosphokinase	2–1,500	299	558
Sodium/potassium ratio		22	24

ALT = alanine aminotransferase; AST = aspartate aminotransferase; BUN = blood urea nitrogen.

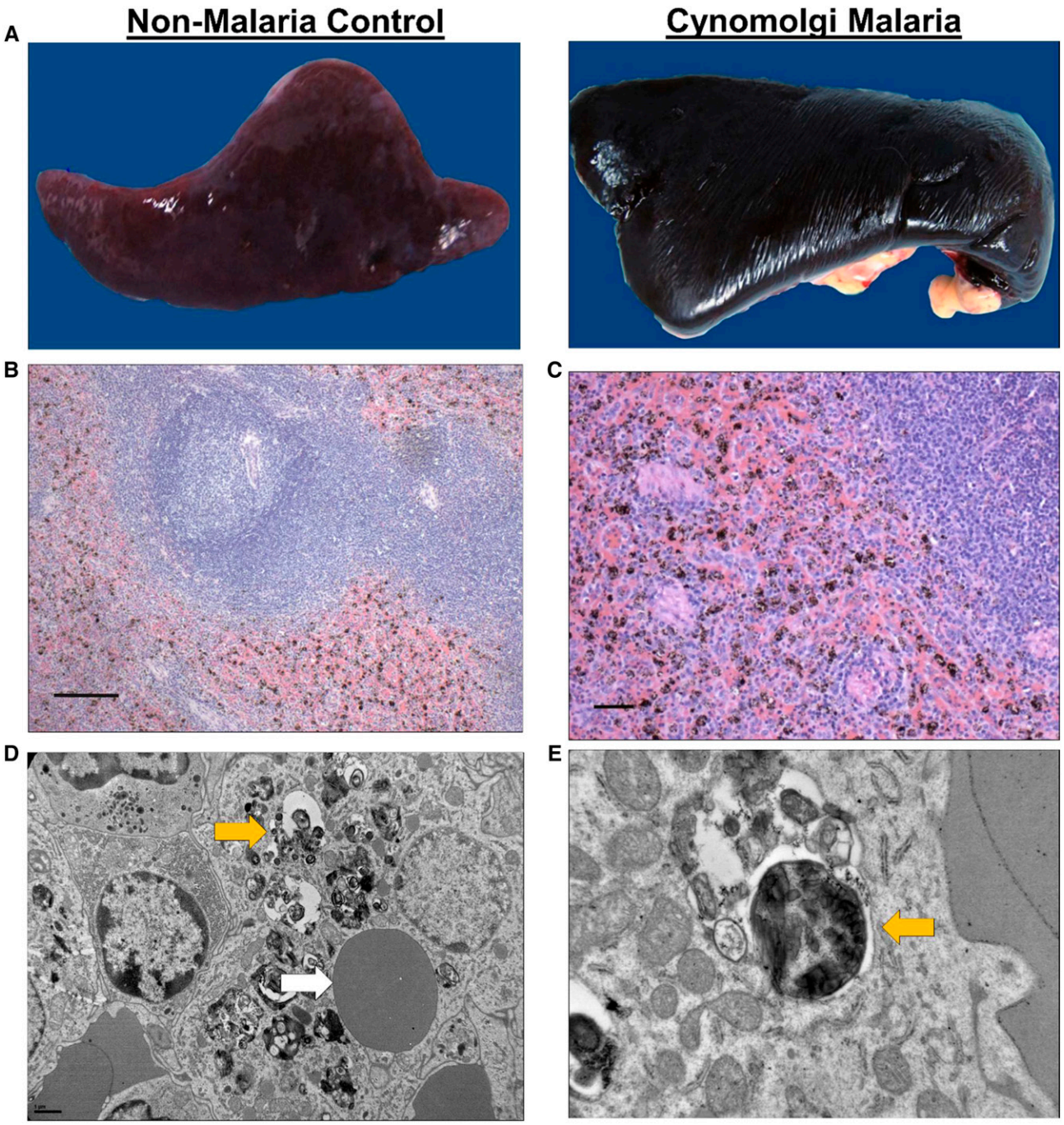

FIGURE 1. Erythrophagocytosis and hemozoin-containing phagocytes in the spleen during severe and complicated cynomolgi malaria. (**A**) Comparison of spleens collected at necropsy from a rhesus macaque with severe and complicated cynomolgi malaria and a rhesus euthanized for reasons other than malaria. (**B** and **C**) Hematoxylin and eosin tissue sections of the spleen from the rhesus with severe and complicated cynomolgi malaria. Notice diffuse deposition of a brown-black pigment consistent with hemozoin. (**D**) Transmission electron micrograph of a spleen depicting a macrophage containing an uninfected red blood cell and hemozoin crystals; yellow arrow = hemozoin, white arrow = uninfected red blood cell. (**E**) Higher magnification of E showing hemozoin contained within a vacuole inside a macrophage; yellow arrow = hemozoin.

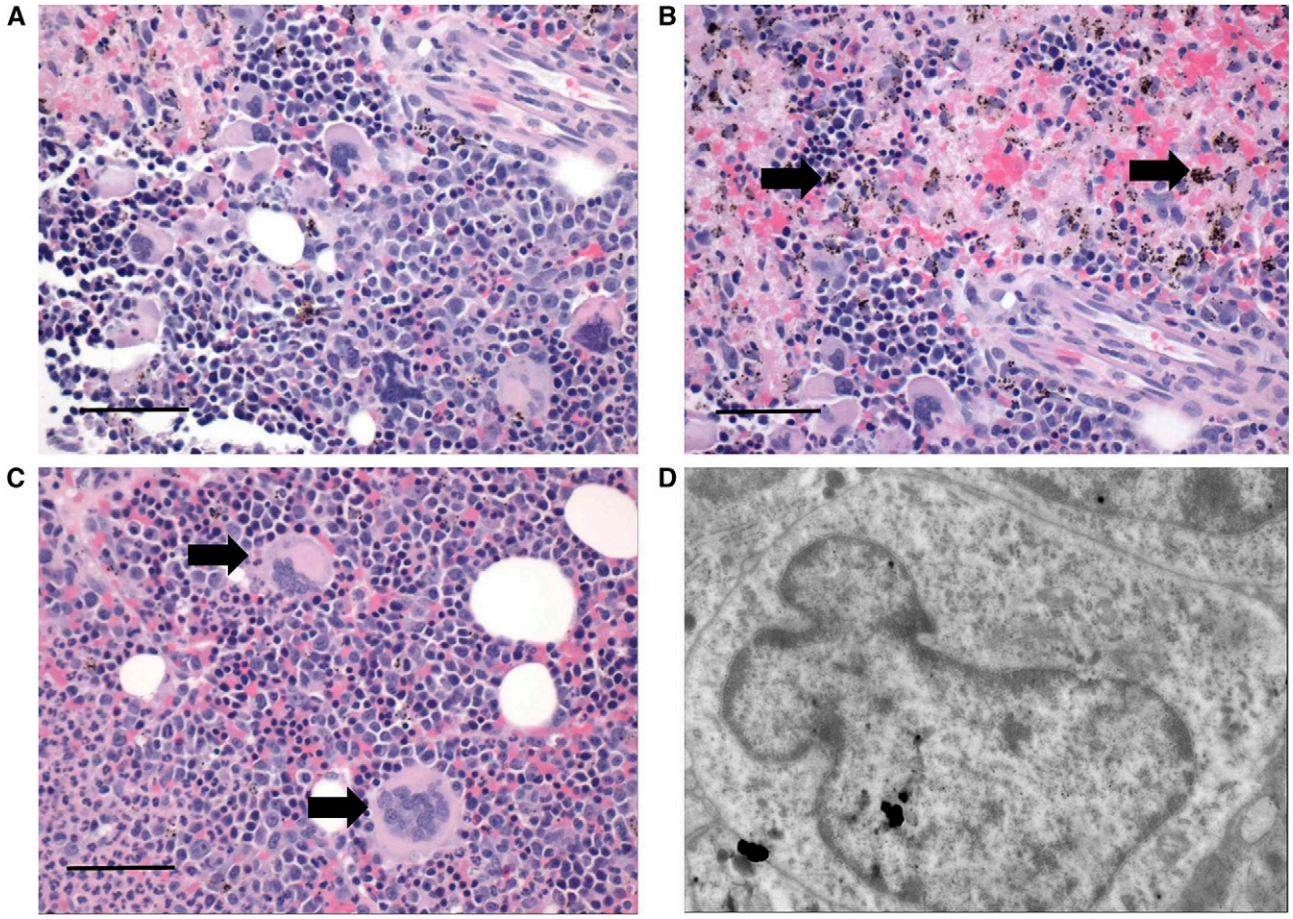

FIGURE 2. Sections of bone marrow during severe and complicated cynomolgi malaria. (**A**, **B**, and **C**) Hematoxylin and eosin stained bone marrow sections from a rhesus macaque with severe and complicated cynomolgi malaria depicting expansion of erythroid precursors and dysplastic megakaryocytes. Panel B: black arrows = hemozoin; Panel C: black arrows = megakaryocytes. (**D**) Transmission electron micrograph of a megakaryocyte from Panel C with an immature, indented nucleus and decreased nucleus to cytoplasm ratio.

(Figure 4A and B). There was mild hemosiderosis, but most pigment was negative for iron stain (Figure 4B).

The kidneys contained many large hypercellular glomeruli, and the renal interstitium was edematous (Figure 5C and E). Interestingly, there were multiple areas with leukocyte infiltrates consisting of plasma cells, lymphocytes, and eosinophils (Figure 5F). The cuboidal epithelium lining renal tubules was eosinophilic and vacuolated (Figure 5C). Many tubules contained cellular and granular casts (Figure 5B) and were lined by cuboidal epithelium that appeared to be undergoing necrosis or apoptosis based on the pyknotic and karyorrhectic morphology of the nuclei (Figure 5C). Mineralization was evident in some tubules (Figure 5D).

DISCUSSION

A case of a rhesus macaque with severe cynomolgi malaria that became complicated by renal failure due to acute tubular necrosis was presented here. This animal's renal function did not improve after antimalarial treatment, intravenous fluid therapy, and blood transfusion, likely due to the severity of the renal dysfunction. Indeed, serum concentrations of creatinine similar to this animal's levels have been associated with poor outcomes in humans.[26] Leukocyte infiltrates composed of plasma cells, eosinophils, and lymphocytes were identified in the kidney, suggesting that these cells may be involved in renal complications.

Hepatic dysfunction was also evident based on hepatomegaly and elevated AST and ALT levels. Interestingly, the liver appeared mostly normal despite evidence of inflammation and leukocyte infiltrates. Hepatocyte degeneration was not observed, as reported in vivax malaria, raising the question whether this finding in humans may be due to other comorbidities in endemic areas.[11]

Respiratory distress is common during complicated vivax malaria, and signs of mild respiratory distress including edema, interstitial pneumonia, type II cell hyperplasia, and fibrin deposition were observed here.[2,12] Parasites were not observed in the lung tissue, unlike previous reports from malaria patients with malaria.[11] This may be because the animal was subcuratively treated 48 hours prior to necropsy. Future studies using the rhesus macaque model could be designed to forego treatment to determine if *P. cynomolgi* predominates in the lungs compared with other organs, as speculated with *P. vivax*.

Macrophages-containing hemozoin were abundant in the spleen, and one macrophage observed by TEM had

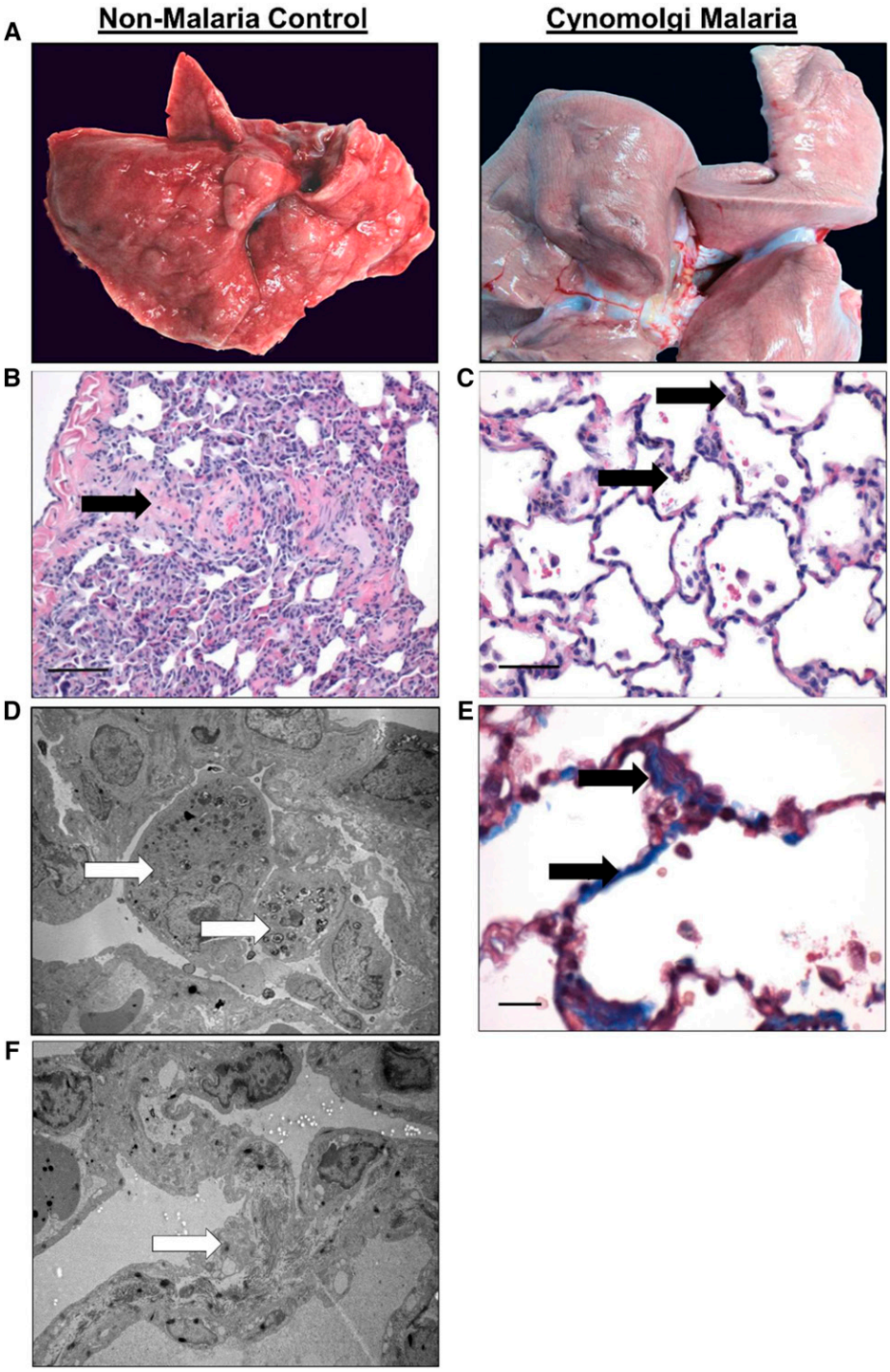

FIGURE 3. Pulmonary lesions during severe and complicated cynomolgi malaria. (**A**) Comparison of a lung collected at necropsy from the rhesus macaque with severe and complicated cynomolgi malaria and a rhesus euthanized for reasons other than malaria. (**B** and **C**) Digital micrographs of sections from Panel A stained with hematoxylin and eosin. Black arrows indicate eosinophilic material in the parenchyma (**B**) and type II cell hyperplasia and alveolar macrophages (**C**). (**D** and **F**) Transmission electron micrographs from the infected lung in Panel A depicting a macrophage-containing hemozoin (**D**) and fibrils contained within type II cells (**F**). (**E**) Lung tissue section stained with Masson's trichrome blue staining. Arrows indicate increased deposition of collagen within the interstitium in the lung.

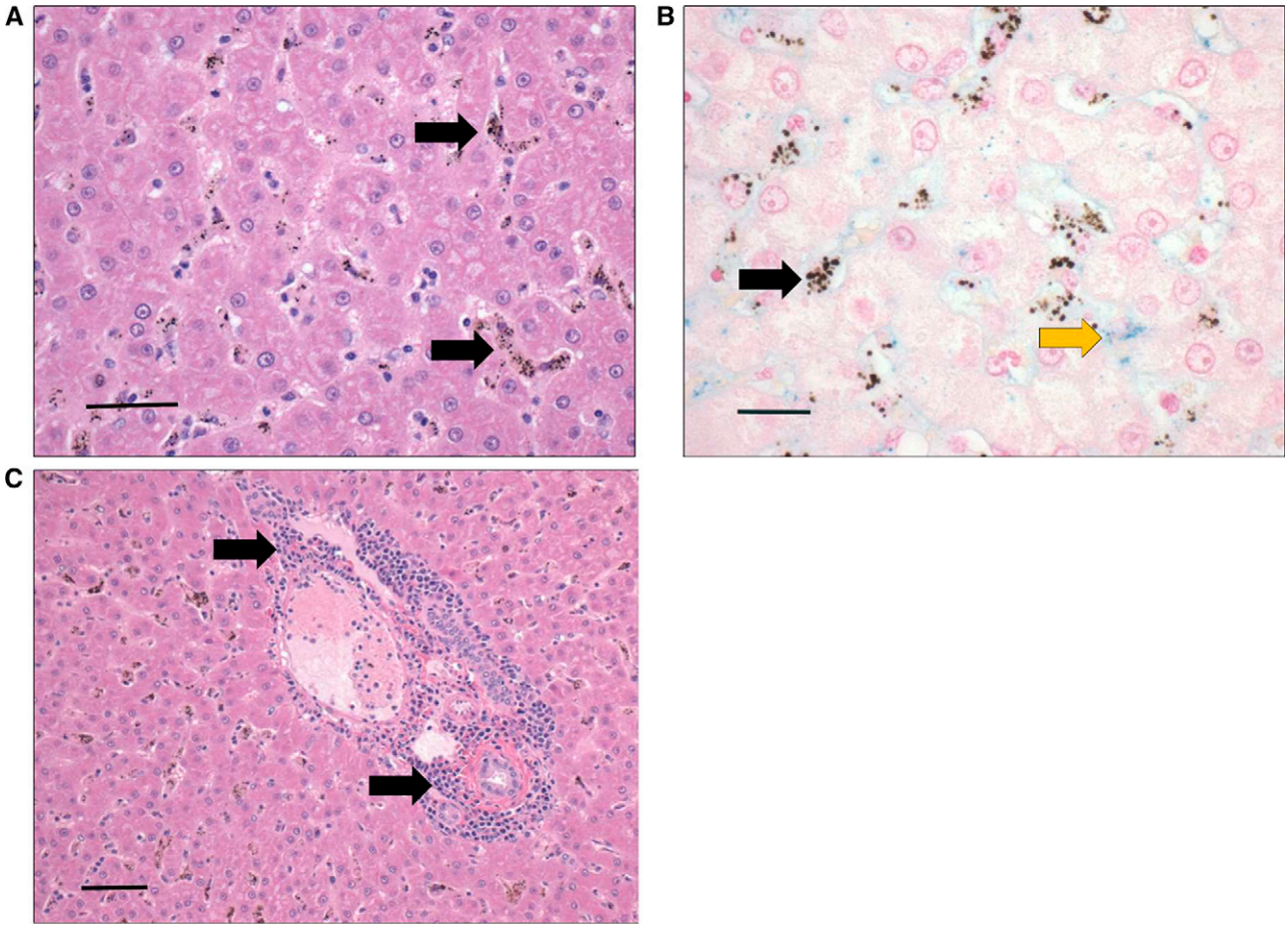

FIGURE 4. Liver section depicting leukocyte infiltrates and hemozoin-laden macrophages lining the sinusoids during severe and complicated cynomolgi malaria. (**A** and **C**) Hematoxylin and eosin stain of liver sections during severe and complicated cynomolgi malaria. (**B**) Liver section stained with Pearl's iron stain depicting blue stain of iron deposits. Panel A: black arrows = hemozoin in phagocytic cells lining the liver sinusoids. Panel B: black arrows = hemozoin; yellow arrow = iron deposits. Panel C: black arrows = lymphoplasmacytic infiltration within portal area.

internalized an uninfected RBC. This finding provides supporting evidence that phagocytosis of uninfected RBCs occurs in vivo.[27–29] Future studies can explore this further using ex vivo samples from carefully timed splenectomies or terminal studies to understand mechanisms relating to the removal of uninfected RBCs.

Alterations in bone marrow morphology were strikingly similar to that reported in humans.[30–32] Myeloid and erythroid cell lineages were markedly increased, hemozoin-containing macrophages were evident throughout the marrow in close proximity to the erythroid series, and megakaryocytes possessed aberrant morphology. This rhesus macaque model enabling multiple bone marrow draws is particularly well-suited for in-depth studies of bone marrow dysfunction and anemia during malaria.

Collectively, the histopathological changes observed here are remarkably similar to severe and complicated malaria in humans. This report supports the use of NHP models to explore malaria pathogenesis and to complement clinical or postmortem studies with human tissues.

Received September 11, 2016. Accepted for publication March 27, 2017.

Published online June 5, 2017.

Acknowledgments: We like to thank John W. Barnwell for helpful discussions and insights related to this case report. Special thanks are also extended to the Yerkes National Primate Research Center veterinary and animal research services staff for their continued support, assistance, and helpful discussions.

Financial support: This project was funded, in part, by Federal funds awarded from the U.S. National Institute of Allergy and Infectious Diseases, National Institutes of Health, Department of Health and Human Services under contract no. HHSN272201200031C (PI: Mary Galinski), which supports the Malaria Host–Pathogen Interaction Center (MaHPIC). Additional support from federal funds was provided by the Office of Research Infrastructure Programs/OD P51OD011132.

Authors' addresses: Chester J. Joyner, Graduate Division of Biological and Biomedical Sciences, Emory University, Atlanta, GA, E-mail: cjjoyne@emory.edu. The MaHPIC Consortium, Yerkes National Primate Research Center, Emory Vaccine Center, Emory University, Atlanta, GA, E-mail: info@mahpic.emory.edu. Jennifer S. Wood, Division of Animal Resources, Yerkes National Primate Research Center, Emory University, Atlanta, GA, E-mail: jennifer.susan.wood@emory.edu. Alberto Moreno, Emory Vaccine Center, Emory University, Atlanta, GA, E-mail: camoren@emory.edu. Anapatricia Garcia, Division of Pathology, Yerkes National Primate Research Center, Emory University, Atlanta, GA, E-mail: ap.garcia@emory.edu. Mary R. Galinski, Department of Medicine, Emory University, Atlanta, GA, and Emory Vaccine Center, Emory University, Atlanta, GA, E-mail: mgalins@emory.edu.

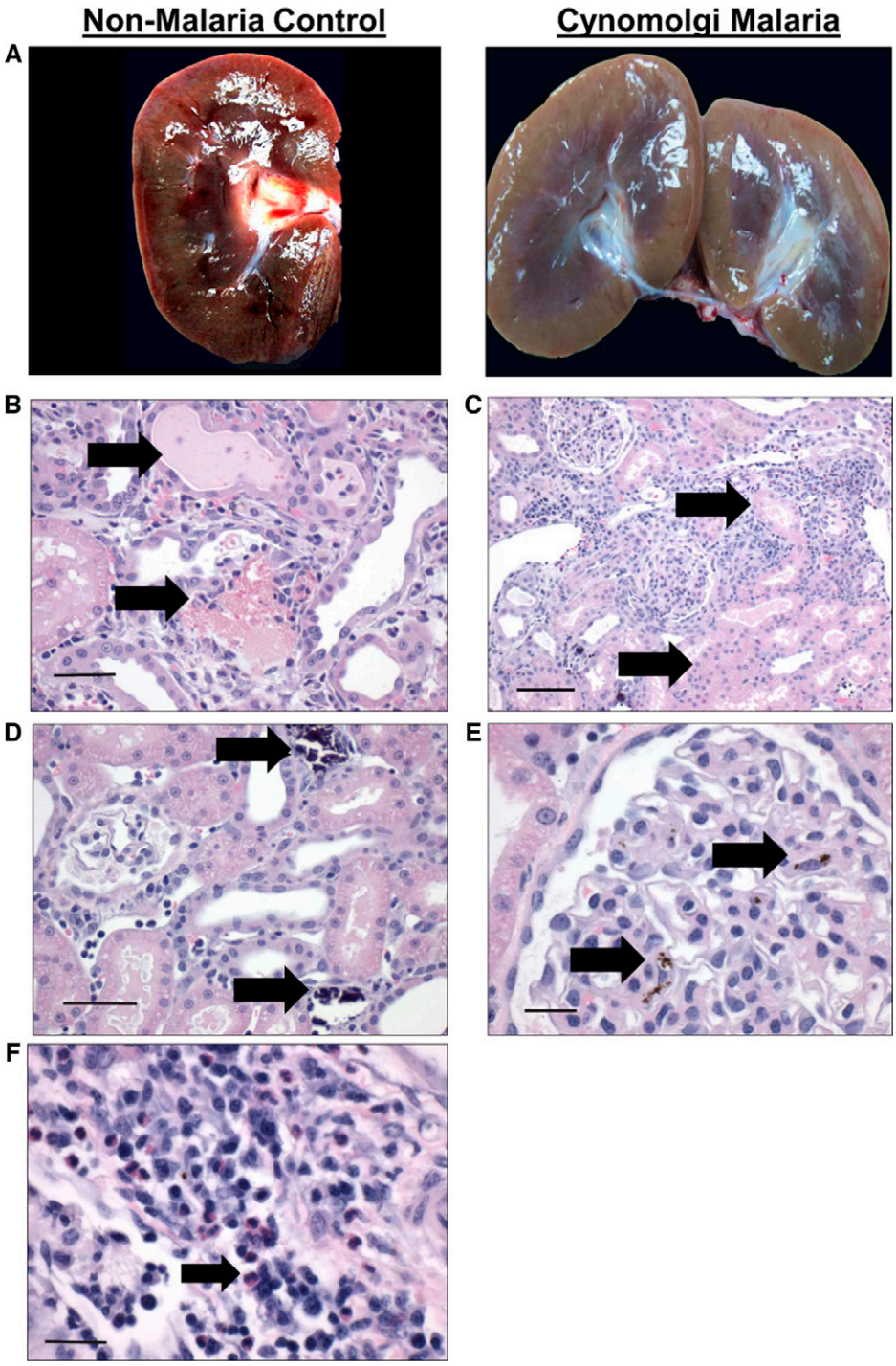

FIGURE 5. Gross and histological findings in the kidney during severe and complicated cynomolgi malaria. (**A**) Comparison of a kidney collected at necropsy from the rhesus macaque with severe and complicated cynomolgi malaria and a rhesus euthanized for reasons other than malaria. (**B**–**F**) Hematoxylin and eosin kidney sections during severe and complicated cynomolgi malaria. Panel B: black arrows = cellular and hyaline casts; Panel C: black arrows = tubules lined with necrotic epithelium; Panel D: black arrows = mineralization in the kidney tubules; Panel E: black arrow = hemozoin in the glomerulus; Panel F: black arrow: inflammatory infiltration of plasma cells, lymphocytes, and eosinophils in the interstitium.

REFERENCES

1. Laishram DD, Sutton PL, Nanda N, Sharma VL, Sobti RC, Carlton JM, Joshi H, 2012. The complexities of malaria disease manifestations with a focus on asymptomatic malaria. *Malar J 11:* 1–15.
2. Anstey NM, Russell B, Yeo TW, Price RN, 2009. The pathophysiology of vivax malaria. *Trends Parasitol 25:* 220–227.
3. Anstey NM, Douglas NM, Poespoprodjo JR, Price RN, 2012. *Plasmodium vivax*: clinical spectrum, risk factors and pathogenesis. *Adv Parasitol 80:* 151–201.
4. Wassmer SC, Taylor TE, Rathod PK, Mishra SK, Mohanty S, Arevalo-Herrera M, Duraisingh MT, Smith JD, 2015. Investigating the pathogenesis of severe malaria: a multidisciplinary and cross-geographical approach. *Am J Trop Med Hyg 93:* 42–56.
5. Joice R, et al., 2014. *Plasmodium falciparum* transmission stages accumulate in the human bone marrow. *Sci Transl Med 6:* 244re5.
6. Hochman SE, et al., 2015. Fatal pediatric cerebral malaria is associated with intravascular monocytes and platelets that are increased with HIV coinfection. *MBio 6:* e01390–e01415.
7. Casals-Pascual C, et al., 2006. Suppression of erythropoiesis in malarial anemia is associated with hemozoin in vitro and in vivo. *Blood 108:* 2569–2577.
8. Lombardini ED, Gettayacamin M, Turner GD, Brown AE, 2015. A review of *Plasmodium coatneyi*-macaque models of severe malaria. *Vet Pathol 52:* 998–1011.
9. Lamikanra AA, Brown D, Potocnik A, Casals-Pascual C, Langhorne J, Roberts DJ, 2007. Malarial anemia: of mice and men. *Blood 110:* 18–28.
10. Langhorne J, et al., 2011. The relevance of non-human primate and rodent malaria models for humans. *Malar J 10:* 23.
11. Lacerda MV, et al., 2012. Postmortem characterization of patients with clinical diagnosis of *Plasmodium vivax* malaria: to what extent does this parasite kill? *Clin Infect Dis 55:* e67–e74.
12. Valecha N, et al., 2009. Histopathology of fatal respiratory distress caused by *Plasmodium vivax* malaria. *Am J Trop Med Hyg 81:* 758–762.
13. Joyner CJ, Barnwell JW, Galinski MR, 2015. No more monkeying around: primate malaria model systems are key to understanding *Plasmodium vivax* liver-stage biology, hypnozoites, and relapses. *Front Microbiol 6:* 145.
14. Galinski MR, Barnwell JW, 2012. Chapter 5, Nonhuman primate models for human malaria research. Abee CR, Mansfield K, Tardif S, Morris T, eds. *Nonhuman Primates in Biomedical Research*, 2nd edition. Boston, MA: Academic Press, 299–323.
15. Joyner C, Moreno A, Meyer EVS, Cabrera-Mora M, Kissinger JC, Barnwell JW, Galinski MR, 2016. *Plasmodium cynomolgi* infections in rhesus macaques display clinical and parasitological features pertinent to modelling vivax malaria pathology and relapse infections. *Malar J 15:* 1–18.
16. Tachibana S, et al., 2012. *Plasmodium cynomolgi* genome sequences provide insight into *Plasmodium vivax* and the monkey malaria clade. *Nat Genet 44:* 1051–1055.
17. Aikawa M, Miller LH, Rabbege J, 1975. Caveola–vesicle complexes in the plasmalemma of erythrocytes infected by *Plasmodium vivax* and *P cynomolgi*. Unique structures related to Schuffner's dots. *Am J Pathol 79:* 285–300.
18. Akinyi S, Hanssen E, Meyer EV, Jiang J, Korir CC, Singh B, Lapp S, Barnwell JW, Tilley L, Galinski MR, 2012. A 95 kDa protein of *Plasmodium vivax* and *P. cynomolgi* visualized by three-dimensional tomography in the caveola-vesicle complexes (Schuffner's dots) of infected erythrocytes is a member of the PHIST family. *Mol Microbiol 84:* 816–831.
19. Warren M, Skinner JC, Guinn E, 1966. Biology of the simian malarias of southeast Asia. I. Host cell preferences of young trophozoites of four species of *Plasmodium. J Parasitol 52:* 14–16.
20. Krotoski WA, Garnham PC, Bray RS, Krotoski DM, Killick-Kendrick R, Draper CC, Targett GA, Guy MW, 1982. Observations on early and late post-sporozoite tissue stages in primate malaria. I. Discovery of a new latent form of *Plasmodium cynomolgi* (the hypnozoite), and failure to detect hepatic forms within the first 24 hours after infection. *Am J Trop Med Hyg 31:* 24–35.
21. Dembele L, et al., 2014. Persistence and activation of malaria hypnozoites in long-term primary hepatocyte cultures. *Nat Med 20:* 307–312.
22. Sutton PL, Luo Z, Divis PC, Friedrich VK, Conway DJ, Singh B, Barnwell JW, Carlton JM, Sullivan SA, 2016. Characterizing the genetic diversity of the monkey malaria parasite *Plasmodium cynomolgi*. *Infect Genet Evol 40:* 243–252.
23. Sheehan D.C. HBB, *Theory and Practice of Histotechnology*. St. Louis, MO: The C.V. Mosby Company.
24. Hayat M, 1986. *Basic Techniques for Transmission Electron Microscopy*. San Diego, CA: Elsevier, Inc.
25. Aurrecoechea C, et al., 2009. PlasmoDB: a functional genomic database for malaria parasites. *Nucleic Acids Res 37:* D539–D543.
26. Sheiban AK, 1999. Prognosis of malaria associated severe acute renal failure in children. *Ren Fail 21:* 63–66.
27. Fonseca LL, Alezi HS, Moreno A, Barnwell JW, Galinski MR, Voit EO, 2016. Quantifying the removal of red blood cells in *Macaca mulatta* during a *Plasmodium coatneyi* infection. *Malar J 15:* 1–15.
28. Jakeman GN, Saul A, Hogarth WL, Collins WE, 1999. Anaemia of acute malaria infections in non-immune patients primarily results from destruction of uninfected erythrocytes. *Parasitology 119:* 127–233.
29. Fernandez-Arias C, et al., 2016. Anti-self phosphatidylserine antibodies recognize uninfected erythrocytes promoting malarial anemia. *Cell Host Microbe 19:* 194–203.
30. Abdalla SH, 1990. Hematopoiesis in human malaria. *Blood Cells 16:* 401–416, discussion 417–419.
31. Wickramasinghe SN, Abdalla SH, 2000. Blood and bone marrow changes in malaria. *Best Pract Res Clin Haematol 13:* 277–299.
32. Knuttgen HJ, 1987. The bone marrow of non-immune Europeans in acute malaria infection: a topical review. *Ann Trop Med Parasitol 81:* 567–576.